Femtosecond laser damage of broadband pulse compression gratings

Fanyu Kong (孔钒宇)[1,2], Yunxia Jin (晋云霞)[1*], Shijie Liu (刘世杰)[1], Shunli Chen (陈顺利)[1,2], Heyuan Guan (关贺元)[1,2], Kai He (何 凯)[1,2], Ying Du (杜 颖)[1,2], and Hongbo He (贺洪波)[1]

[1] *Key Laboratory of Materials for High Power Laser, Shanghai Institute of Optics and Fine Mechanics, Chinese Academy of Sciences, Shanghai 201800, China*

[2] *University of Chinese Academy of Sciences, Beijing 100049, China*

[*] *Corresponding author: yxjin@siom.ac.cn*

Received March 29, 2013; accepted August 8, 2013; posted online September 29, 2013

The fabricated gratings used for an 800-nm compressed laser pulse have more than 90% diffraction efficiency in the –1st order for TE polarization within 760–860 nm, and the maximum value is 94.3%. The laser-induced damage threshold (LIDT) of the gratings increases from 0.53 to 0.75 J/cm^2 in the normal beam in a pulse width τ of 40–100 fs. The LIDT of the gratings is observed a $\tau^{0.25}$ scaling in the pulse width region. The damage morphologies of the gratings indicate that the initial damage of the gratings locates at the grating lines, a position that coincides with that of the electric field maximum.

OCIS codes: 230.1950, 320.2250, 320.5520.

doi: 10.3788/COL 201311.102302.

Diffraction gratings are vital components in the compressor of a high-power chirped pulse amplification (CPA) laser system[1]. The CPA technique uses one or more gratings in a "stretcher" to temporally disperse a low-energy, broadband, short-pulse beam. The stretched beam is then amplified without undergoing nonlinear self-focusing. The amplified, stretched pulse is finally sent through a "compressor" that typically contains two to four gratings to create an intense pulse of nearly the initial pulse duration[2]. The conditions for grating that allow only reflection into the 0 and –1 orders are summarized under so-called classical mounting. Therefore, the grating is optimized with all diffraction orders in the transmission and reflection vanish exception of the diffracted –1 order[3–5]. A multilayer dielectric grating (MDG) is first proposed in 1991 as a possible solution to increase the damage threshold and maximize average power operation; therefore, the gratings operating at a centered wavelength $\lambda \approx 1$ μm have been fabricated and included in numerous studies[4,6,7]. With the development of an ultrashort pulse laser system that operates in the 800-nm wavelength range[8], the diffraction gratings used in ultrashort pulse compression have emerged and been examined[5,9–12]. The gratings for ultrashort pulse compression must meet the basic performance requirements of high efficiency, adequate bandwidth, and high laser damage resistance[10]. Because of the inherent absorption loss of metals, the performance of metal gratings is limited, even though they provide a broad, quasi-top-hat diffraction efficiency spectrum (over 200 nm wide) for TM polarization[5]. Although MDG can offer high laser damage resistance, obtaining a 100-nm bandwidth has always been a challenge. In 2007, Lyndin *et al.* reported their results on all-dielectric HfO_2 gratings with 96% diffraction efficiency over a bandwidth of 38 nm and a high damage threshold of 1.1 J/cm^2 for 50 fs[9–11]. Martz *et al.* (2009) reported an aperiodic $(Nb_{0.5}Ta_{0.5})_2O_5$-SiO_2 broadband MDG centered at 800 nm with a diffraction efficiency of 96% between 780- and 820-nm wavelength and 0.4 ± 0.02 J/cm^2 damage threshold for 120 fs[12]. In 2010, our group reported a 110-nm bandwidth design result of the MDG on the basis of a simulated annealing algorithm and the Fourier mode method to increase bandwidth[5]. The gratings used for an 800-nm femtosecond pulse compression were designed to have a line density of 1960 lines/mm etched in the HfO_2 top layer of a dielectric high-reflectivity (HR) mirror. The HR mirror was composed of an alternate Ta_2O_5/SiO_2 layer and an HfO_2 top layer[13]. The MDG has more than 97% flat-top diffraction efficiency in the –1st order TE polarization over a 110-nm wavelength range around a wavelength of 800 nm. The schematic diagram of the MDG is shown in Fig. 1. In Fig. 1, t_1, t_2, t_m, t_r, t_g, f, Λ, and θ represent H(Ta_2O_5) thickness, L(SiO_2) thickness, match layer thickness, residual layer thickness, groove depth, fill factor, period, and grating profile base angle, respectively.

Based on the design parameters, the HR mirror was deposited on a fused silica substrate (50 × 50 (mm)) by electron beam evaporation. The mirror has a more than

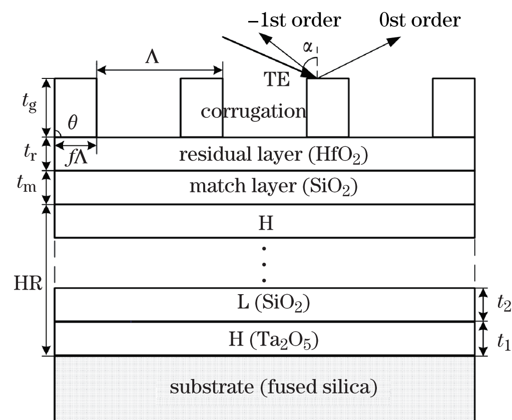

Fig. 1. Schematic of the multilayer dielectric grating.

 © 2013 Chinese Optics Letters

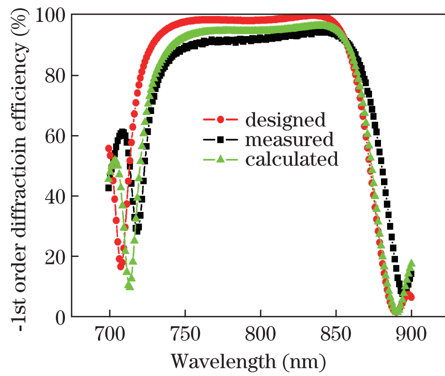

Fig. 2. (Color online) Designed, measured, and calculated –1st order diffraction efficiency curves.

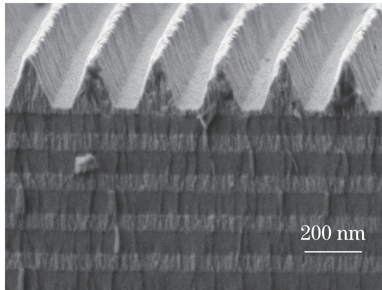

Fig. 3. SEM image of the MDG.

Table 1. Measured Parameters of the MDG

Parameter	t_1 (nm)	t_2 (nm)	t_m (nm)	t_r (nm)	t_g (nm)	Λ (nm)	f	θ (deg.)
Value	101.8	146.4	120	146	233	510	0.5	69

160-nm bandwidth (reflectance > 99%) around a wavelength of 800 nm and 83% transmission at the exposure wavelength of 413 nm[13]. The grating structures were fabricated by the Laboratory of Gratings and Measurement, Department of Precision Instrument, Tsinghua University. The −1st order diffraction efficiency of the MDG was measured several times over the entire area of the sample with the use of the scanning photometry tool detailed in Ref. [14]. Figure 2 shows that the mean measured −1st order diffraction efficiency for the TE polarization wavelength from 760 to 860 nm is 92%, and the maximum value is 94.3% at 845 nm. Figure 3 shows that the grating structure is observed in detail with scanning electron microscopy (SEM, model: Zeiss Auriga). SEM features a Schottky field emission Gemini electron column that operates between 100 V and 30 kV and is capable of resolutions of 1.0 nm at 15 kV and 1.9 nm at 1 kV. Figure 3 shows that no visible etching residue on the surface and in the groove bottom can be observed, and the structure of the grating is shaped like a trapezoid. The parameters of the grating structure combined with layer thickness were measured and listed in Table 1. These parameters were used to accurately calculate the −1st order diffraction efficiency and bandwidth of the MDG with our software developed in the framework of the Fourier mode method[9]. The calculated spectrum curve shown in Fig. 2 is consistent with the measured result.

The experimental setup for the damage test (Fig. 4) involves an 800-nm CPA Ti: sapphire laser system that produces a near-Gaussian spatial profile compressed P-polarized pulse with up to 3.8-mJ energy. The pulse duration is continuously varied in the range of 38–100 fs. The system can be run at a repetition rate of approximately 1 kHz. A half-wave plate works to vary the pulse from P-polarized to S-polarized. The attenuator is used to adjust the irradiation energy in the samples. An isolated mechanical shutter is used to obtain a different pulse number. Beam diagnostics is used to monitor the spot morphology of each pulse. The pulse energy is measured by an energy meter from a split-off portion of the beam. The Gaussian spatial spot, with an area of $\sim 1.37\times 10^{-2}$ mm^2 in the normal beam, can be achieved in the focal plane of a lens with a focal length of 50 cm. The sample for the damage test is mounted on a motorized x-y translation stage. The sample is monitored *in situ* with a charge-coupled device (CCD) and He/Ne laser to avoid heating the sample. The entire apparatus is automatically manipulated by a computer. The system error is ±10%.

The MDG samples were utilized in damage tests in the pulse width of 40–100 fs at the facility. In the test procedure, every damage test site was exposed to one laser pulse. Ten sites were irradiated by the same laser fluence. The fluence was gradually decreased until no damage occurred. The irradiated sites were initially assessed for damage with the aid of the CCD. After the damage tests, a Leica DMR polarizing microscope (100×) was used to determine the site damage and to measure the size of the damaged sites. The LIDT ($F_{\rm th}$) of the samples can be obtained by linear extrapolation method (damage area→0) in Gaussian spots because the damage area and the logarithm of fluence in the femtosecond region have a linear relationship[15]. Figure 5(a) shows that the measured LIDT ($F_{\rm th}$) in the normal beam of MDG increased

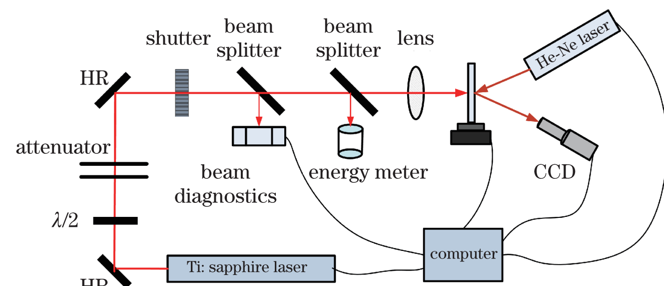

Fig. 4. Experimental setup for the damage test.

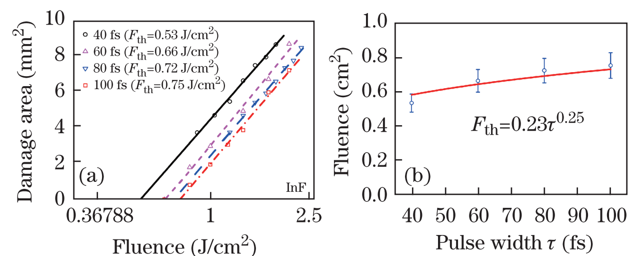

Fig. 5. (Color online) (a) Fitting lines of damage area versus the logarithm of fluence in a pulse width from 40 to 100 fs; (b) relationship between the LIDT between the MDG and pulse width.

from 0.53 to 0.75 J/cm^2 for a pulse width of 40–100 fs. Comparison of the fitting lines shows that the shorter pulse caused serious damage on the MDG under the same irradiation fluence condition. With a system error of 10% considered, the LIDT of the MDG in this pulse width region observed a $\tau^{0.25}$ scaling, as shown in Fig. 5(b). The index (0.25) is not only less than that in a variety of pure and multilayer dielectric materials ($\tau^{0.3-0.6}$) from 20 s to over 100 ps[16] but is also less than that in 1 053-nm pulse compression gratings ($\tau^{0.265}$) from 0.66 to 9.7 ps[17]. These results indicate that the index should be on a declining trend with the decrease in pulse width.

The typical damage morphologies of the MDG were observed in detail with SEM (Fig. 6). The morphologies show that damages only appear in the grating layer, as depicted in Figs. 6(a)–(d). The damaged area of the MDG as a result of the laser pulse decreases in size along with the increase in pulse width. This result implies that the short pulse creates a large damage area in the same irradiation fluence. Figures 6(a')–(d') shows the amplified image of the rectangular area in Figs. 6(a)–(d), respectively. The detailed damage characteristic demonstrates that all the initial damages occur on the grating lines at the opposite side of the illuminating beam. The damage of the grating lines with no distinct melting phenomenon shows that the melting process is not the main reason for the damage in the ultrashort range. To our knowledge, a femtosecond pulse-induced initial damage of a dielectric is a nonlinear damage process. The electric field intensity is also a very important factor for the nonlinear absorption process[18]. The parameters of the grating structure (Table 1) were accurately measured to calculate the normalized electric field intensity (NEFI) distribution of the MDG and intuitively explain the

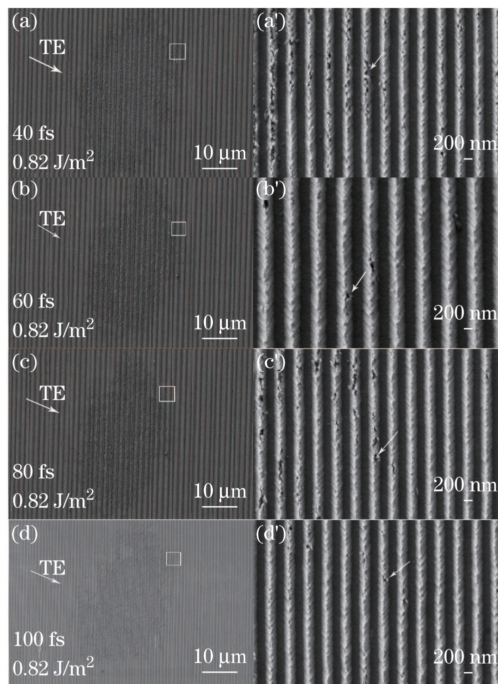

Fig. 6. Typical damage morphology of the MDG in a pulse width from 40 to 60 fs. (a)–(d) show the panorama of the damage from 40 to 100 fs. (a')–(d') show the detailed damage morphologies of the damage edges in (a)–(d), respectively.

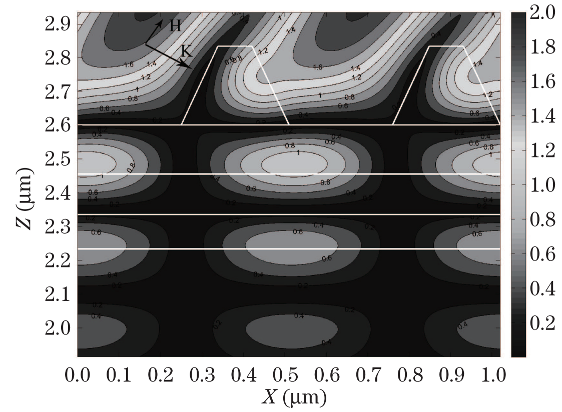

Fig. 7. Near-field distribution of the manufactured MDG. TE polarization laser with the incidence angle of 57° coming from the left.

initial damage. The NEFI distribution is calculated with the TE polarization laser at a wavelength of 800 nm coming from the left at an incident angle of 57°. The distribution shown in Fig. 7 demonstrates that the electric field maximum is located on the grating ridge at the opposite side of the illuminating beam. Combining Figs. 6 and 7 indicates that the damage begins on the grating lines at the opposite side of the illuminating beam where the enhancement of the electric field is maximum. This microscopic observation proves the link between the maximum electric field and damage initiation. Therefore, decreasing the electric field intensity maximum by optimization of the parameters of the grating structure is one of the primary methods to increase laser damage resistance of the MDG.

In conclusion, the manufactured MDG has more than 90% flat-top diffraction efficiency in the −1st order for TE polarization with a 100-nm bandwidth around 800 nm. The LIDT of the MDG increases from 0.53 to 0.75 J/cm^2 pulse width from 40 to 100 fs, which observes a $\tau^{0.25}$ scaling in the pulse width range. Basing from the analysis of damage morphology and the NEFI distribution, we consider that the local enhancement of the electric field intensity in a dielectric grating ridge relates directly to the laser damage resistance of the multilayer dielectric grating.

This work was supported by the National "863" Program of China and the National Natural Science Foundation of China (Nos. 10704079 and 11104295). The authors wish to thank the Laboratory of Gratings and Measurement, Department of Precision Instrument, Tsinghua University for the fabrication of the grating structure and Professor Yuxin Leng's group in the Shanghai Institute of Optics and Fine Mechanics for offering the laser source. The authors also express their gratitude to Professor Zhengxiu Fan for the useful discussion on this work and Dr. Yun Cui for the SEM measurements.

References

1. N. Blanchot, G. Behar, T. Berthier, E. Bignon, F. Boubault, C. Chappuis, H. Coic, C. Damiens-Dupont, J. Ebrardt, Y. Gautheron, P. Gibert, O. Hartmann, E. Hugonnot, F. Laborde, D. Lebeaux, J. Luce, S. Montant, S. Noailles, J. Néauport, D. Raffestin, B. Remy, A. Roques, F. Sautarel, M. Sautet, C. Sauteret, and C.

Rouyer, Plasma Phys. Contr. Fusion **50,** 124045 (2008).
2. J. Britten, "Diffraction gratings for high-intensity laser applications," Lawrence Livermore National Laboratory, Livermore, LLNL-BOOK-401125 (2008).
3. K. Hehl, J. Bischoff, U. Mohaupt, M. Palme, B. Schnabel, L. Wenke, R. Bödefeld, W. Theobald, E. Welsch, R. Sauerbrey, and H. Heyer, Appl. Opt. **38,** 6257 (1999).
4. J. Wang, Y. Jin, S. Liu, J. Shao, and Z. Fan, Chin. Opt. Lett. **8,** 29 (2010).
5. J. Wang, Y. Jin, J. Shao, and Z. Fan, Opt. Lett. **35,** 187 (2010).
6. J. Neauport, E. Lavastre, G. Razé, G. Dupuy, N. Bonod, M. Balas, G. de Villele, J. Flamand, S. Kaladgew, and F. Desserouer, Opt. Express **15,** 12508 (2007).
7. J. Qiao, A. W. Schmid, L. J. Waxer, T. Nguyen, J. Bunkenburg, C. Kingsley, A. Kozlov, and D. Weiner, Opt. Express **18,** 10423 (2010).
8. A. Ostendorf, T. Bauer, F. Korte, J. R. Howorth, C. Momma, N. H. Rizvi, F. Saviot, and F. Salin, Proc. SPIE **4633,** 128 (2002).
9. N. Lyndin, M. Flury, S. Tonchev, R. Fechner, and O. Parriaux, J. Eur. Opt. Soc-Rapid **2,** 07019 (2007).
10. F. Canova, R. Clady, J. Chambaret, M. Flury, S. Tonchev, R. Fechner, and O. Parriaux, Opt. Express **15,** 15324 (2007).
11. M. Flury, S. Tonchev, R. Fechner, A. Schindler, and O. Parriaux, J. Eur. Opt. Soc-Rapid **2,** 0724(2007).
12. D. H. Martz, H. T. Nguyen, D. Patel, J. A. Britten, D. Alessi, E. Krous, Y. Wang, M. A. Larotonda, J. George, B. Knollenberg, B. M. Luther, J. J. Rocca, and C. S. Menoni, Opt. Express **17,** 23809 (2009).
13. F. Kong, S. Chen, S. Liu, Y. Jin, H. Guan, Y. Du, C. Wei, H. He, and K. Yi, Proc. SPIE **8206,** 82060P (2012).
14. K. He, J. Wang, Y. Hou, X. Li, H. Guan, F. Kong, S. Liu, Y. Jin, and K. Yi, Appl. Opt. **52,** 653 (2013).
15. P. Balling and J. Schou, Rep. Prog. Phys. **76,** 036502 (2013).
16. B. C. Stuart, M. D. Feit, A. M. Rubenchik, B. W. Shore, and M. D. Perry, Phys. Rev. Lett. **74,** 2248 (1995).
17. F. Kong, Y. Jin, D. Li, W. Chen, M. Zhu, T. Wang, C. Li, H. He, G. Xu, and J. Shao, Proc. SPIE **8530,** 85300L (2012).
18. S. Chen, Y. Zhao, H. He, and J. Shao, Chin. Opt. Lett. **9,** 083101 (2011).